Antiresonance induced by symmetry-broken contacts in quasi-one-dimensional lattices

Jung-Wan Ryu, Nojoon Myoung, and Hee Chul Park[*]

Center for Theoretical Physics of Complex Systems, Institute for Basic Science (IBS), Daejeon 34051, Republic of Korea

We report the effect of symmetry-broken contacts on quantum transport in quasi-one-dimensional lattices. In contrast to one-dimensional (1D) chains, transport in quasi-one-dimensional lattices, which are made up of a finite number of 1D chain layers, is strongly influenced by contacts. Contact symmetry depends on whether the contacts maintain or break the parity symmetry between the layers. With balanced on-site potential, a flatband can be detected by asymmetric contacts, but not by symmetric contacts. In the case of asymmetric contacts with imbalanced on-site potential, transmission is suppressed at certain energies. We elucidate these energies of transmission suppression related to antiresonance using reduced lattice models and Feynman paths. These results provide a nondestructive measurement of flatband energy, which is difficult to detect.

I. INTRODUCTION

Quantum dots are often referred to as artificial atoms, as their electrons are confined in all spatial dimensions with discretized energy [1,2]. Likewise, coupled quantum dots can be considered as artificial molecules or crystals [3–5]. Quantum dot arrays are accordingly a promising candidate for artificial lattices, which have attracted a great deal of attention recently considering their relation to not only fundamental physics but also various potential applications, e.g., quantum computation, spintronics, engineering of energy bands, and topological states in non-Hermitian lattices [6–13]. The electronic states in ideal arrays of uniform quantum dots can be described by discrete-level representations, such as the tight-binding model [14,15], and electronic transport in quantum dot arrays has been studied extensively as the electronic states can be probed when coupling is allowed between dots and leads. In the presence of a defect, transport shows antiresonance where the transmission probability vanishes [16–19]; in other words, the conducting channel is completely blocked by the defect when the Fermi energy is right at the defect energy level.

Apart from a one-dimensional chain of quantum dots, quasi-one-dimensional (quasi-1D) lattices have revealed peculiar electronic states, such as flatbands. Flatband lattice models where at least one band is completely flat over the whole momentum space—implying zero dispersion—have attracted considerable interest from various areas, including superconductors [20–23], optical and photonic lattices [24–28], and exciton-polariton condensates [10,29]. The simplest flatband lattice models are quasi-1D lattices that have translational symmetry in the infinite longitudinal direction and parity symmetry in a finite transverse direction, for example cross-stitch and tunable diamond lattices. In these lattices, the flatbands and dispersive bands are completely decoupled because they have odd- and even-parity symmetric eigenstates, respectively. The odd symmetry of the flatbands produces compact localized eigenstates with nonzero amplitude only at a finite number of lattice sites due to destructive interference [30–33].

In this work, we study quantum transport in quasi-1D lattices with symmetric and asymmetric contacts, which, in contrast to transport in 1D chains, strongly influence transport in quasi-1D lattices. Imperfect contacts between system and leads can be considered as defects that break the symmetries of the lattice. We consider two cases according to the existence of flatbands related to the balance of on-site potential. First, when a quasi-1D lattice has flatbands due to balanced on-site potential, it is natural that transport does not reflect flatbands as the compact localized states in the flatbands are such that they are unavailable for charge transfer. We show, however, that flatbands can be detected by symmetry-broken contacts, but not by symmetric contacts. Next, in quasi-1D lattices with imbalanced on-site potential, although there are no flatbands, transmission has additional dips irrespective of the energy bands in the case of asymmetric contacts. We explain the energies of this transmission suppression related to antiresonance using reduced lattice models and Feynman paths.

This paper is organized as follows. In Sec. II we describe the energy bands and quantum transport in quasi-1D lattices with flatbands. The results of transmission in lattices without flatbands due to imbalanced on-site potential are presented in Sec. III, and in Sec. IV we summarize our results.

II. QUASI-ONE-DIMENSIONAL LATTICES—FLATBAND LATTICES

A. Cross-stitch lattices

In this section, we study the energy bands and quantum transport in two quasi-1D lattices: a cross-stitch and a tunable diamond lattice. Figure 1 illustrates the cross-stitch and tunable diamond lattices. The Schrödinger equation of a quasi-1D flatband lattice is given by

$$E\Psi_j = H_0\Psi_j + H_1\Psi_{j+1} + H_1^+\Psi_{j-1}, \quad (1)$$

where H_0 is the on-site energy matrix and H_1 is the nearest-neighbor hopping matrix. The tight-binding Hamiltonian for a cross-stitch lattice is given by

$$H_0 = \begin{pmatrix} \epsilon_a & -t \\ -t & \epsilon_b \end{pmatrix}, \quad H_1 = \begin{pmatrix} -d & -d \\ -d & -d \end{pmatrix}, \quad (2)$$

where $\Psi_j = (a_j b_j)^T$. On-site potential energies are ϵ_a and ϵ_b, respectively, and hopping strengths between the two sites are d
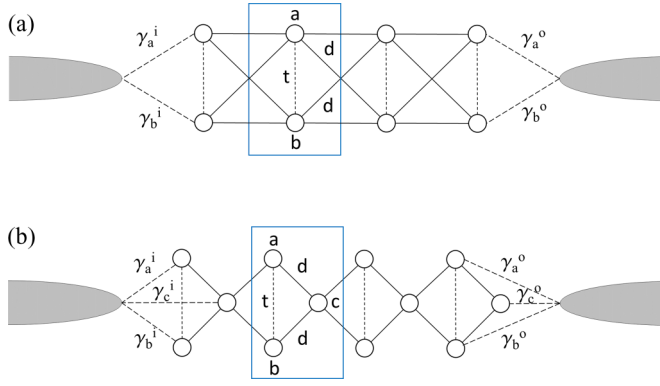
---
[*]hcpark@ibs.re.kr

FIG. 1. (a) Cross-stitch lattice with two leads. Blue rectangular boxes represent unit cells. The unit cell has two sites, a and b, with hopping strengths d (solid lines) and t (dashed line) between the sites. The coupling between sites and leads is $\gamma_{a(b,c)}^{i(o)}$ (long-dashed line). (b) Tunable diamond lattice with two leads. The unit cell has three sites, a, b, and c, with hopping strengths d (solid lines) and t (dashed line) between sites.

and t. We can set $\Psi_{j+1} = \Psi_j e^{ik}$ and $\Psi_{j-1} = \Psi_j e^{-ik}$ because of the translational symmetry of the unit cells. Finally, the Hamiltonian for the cross-stitch lattice is given by

$$H = \begin{pmatrix} \epsilon_a - 2d\cos k & -t - 2d\cos k \\ -t - 2d\cos k & \epsilon_b - 2d\cos k \end{pmatrix}. \tag{3}$$

Solving the eigenproblem of H when $\epsilon_a = \epsilon_b = 0$, we obtain the energy bands for the cross-stitch lattice as

$$E(k) = -t - 4d\cos k, \quad E_{\text{FB}} = t, \tag{4}$$

where $E(k)$ and E_{FB} are dispersive and flatband energies, respectively. Figure 2(a) shows the dispersive and flatbands when $t = d = 1$.

Here, we discuss quantum transport in the quasi-1D lattices. The system under study is composed of a cross-stitch or a tunable diamond lattice with N unit cells, as shown in Fig. 1, with two leads connected to the left and right end unit cells. The Hamiltonian of this system is given by

$$H = H_{\text{Q1D}} + H_{\text{lead}} + H_{\text{coupling}}, \tag{5}$$

where H_{Q1D}, H_{lead}, and H_{coupling} describe the quasi-1D lattice, leads, and coupling between the lattice and leads, respectively, and are given by

$$H_{\text{Q1D}} = \sum_{i=1}^{N} H_0 d_i^\dagger d_i + \sum_{i=1}^{N-1} (H_1 d_{i+1}^\dagger d_i + \text{H.c.}), \tag{6}$$

$$H_{\text{lead}} = -\frac{V_0}{2} \sum_{j \neq 0} (c_{j+1}^\dagger c_j + \text{H.c.}), \tag{7}$$

$$H_{\text{coupling}} = G^i d_1^\dagger c_{-1} + G^o d_N^\dagger c_1 + \text{H.c.}, \tag{8}$$

where $d_j^\dagger$ (d_j) and $c_j^\dagger$ (c_j) are electron creation (annihilation) operators for the lattice and leads, respectively. $V_0/2$ is hopping strength in the leads, and $G^{i(o)}$ describes the
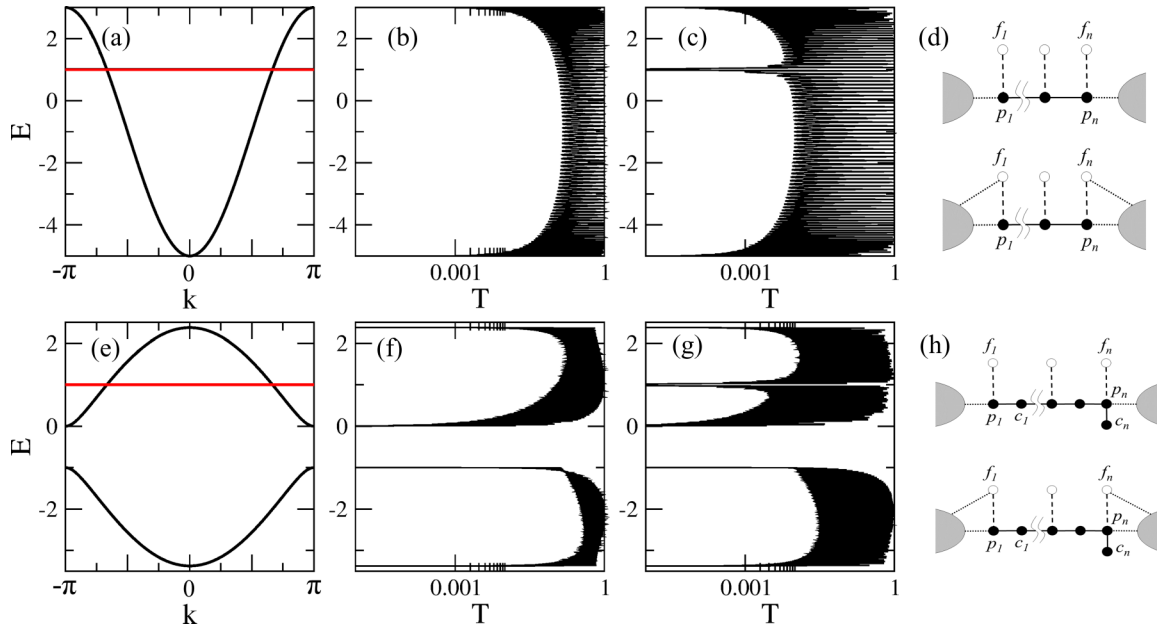
FIG. 2. (a) Energy bands for a cross-stitch lattice with a flatband (red line). (b) Transmission probabilities for a cross-stitch lattice of which both a and b sites of the end unit cells are connected to the input and output leads. (c) Transmission probabilities for a cross-stitch lattice of which only the a sites of the end unit cells are connected to the input and output leads. (d) Upper and lower panels show detangled Fano lattices from a cross-stitch lattice with symmetric and asymmetric contacts, respectively, corresponding to (b) and (c). The hopping strength (dashed lines) between Fano states f_n and dispersive chain p_n equals zero. (e) Energy bands for a tunable diamond lattice with a flatband (red line). (f) Transmission probabilities for a tunable diamond lattice of which both a and b sites of the end unit cells are connected to the input and output leads. (g) Transmission probabilities for a tunable diamond lattice of which only the a sites of the end unit cells are connected to the input and output leads. (h) Upper and lower panels show detangled Fano lattices from a tunable diamond lattice with symmetric and asymmetric contacts, respectively, corresponding to (f) and (g).

coupling between the lattice and the left (right) lead. The amplitude equations of the total Hamiltonian of Eq. (5) can be written as

$$E\phi_{-1} = -\frac{V_0}{2}\phi_{-2} + G^{i^T}\Psi_1, \tag{9}$$

$$E\Psi_1 = H_0\Psi_1 + H_1\Psi_2 + \phi_{-1}G^i, \tag{10}$$

$$E\Psi_j = H_0\Psi_j + H_1^\dagger\Psi_{j-1} + H_1\Psi_{j+1}\ (2 \leqslant j \leqslant N-1), \tag{11}$$

$$E\Psi_N = H_0\Psi_N + H_1^\dagger\Psi_{N-1} + \phi_1 G^o, \tag{12}$$

$$E\phi_1 = -\frac{V_0}{2}\phi_2 + G^{o^T}\Psi_N, \tag{13}$$

where

$$\phi_j = e^{iqj} + re^{-iqj}\quad (j < 0), \tag{14}$$

$$= te^{iqj}\qquad\quad (j > 0). \tag{15}$$

ϕ_j represents the jth sites of leads, and $G^{i\,(o)}$ is given by

$$G^{i\,(o)} = \begin{pmatrix} -\gamma_a^{i\,(o)} \\ -\gamma_b^{i\,(o)} \end{pmatrix}. \tag{16}$$

r and t are reflection and transmission coefficients, respectively, and $|r|^2 + |t|^2 = 1$ in Hermitian cases. Finally, we obtain the equations as follows:

$$-\frac{V_0}{2} = \frac{V_0}{2}r + G^{i^T}\Psi_1, \tag{17}$$

$$-e^{-iq}G^i = e^{iq}rG^i + (H_0 - E)\Psi_1 + H_1\Psi_2, \tag{18}$$

$$0 = H_1^\dagger\Psi_{j-1} + (H_0 - E)\Psi_j + H_1\Psi_{j+1}, \tag{19}$$

$$0 = H_1^\dagger\Psi_{N-1} + (H_0 - E)\Psi_N + e^{iq}tG^o, \tag{20}$$

$$0 = \frac{V_0}{2}t + G^{o^T}\Psi_N, \tag{21}$$

where the energy of the leads is given by $e^{\pm iq} = -E/V_0 \pm i\sqrt{1 - |E/V_0|^2}$. Finally, we can obtain R and T for the cross-stitch lattice from the following equation:

$$\begin{pmatrix} -\frac{V_0}{2} \\ -e^{-iq}G^i \\ 0 \\ \vdots \\ 0 \\ 0 \\ 0 \end{pmatrix} = \begin{pmatrix} \frac{V_0}{2} & G^{i^T} & & & & & \\ e^{iq}G^i & H_0 - EI & H_1 & & & & \\ & H_1^\dagger & H_0 - EI & H_1 & & & \\ & & \ddots & \ddots & \ddots & & \\ & & & H_1^\dagger & H_0 - EI & H_1 & \\ & & & & H_1^\dagger & H_0 - EI & e^{iq}G^o \\ & & & & & G^{o^T} & \frac{V_0}{2} \end{pmatrix} \begin{pmatrix} r \\ \Psi_1 \\ \Psi_2 \\ \vdots \\ \Psi_{N-1} \\ \Psi_N \\ t \end{pmatrix}. \tag{22}$$

Hamiltonians H_0 and H_1 are 2×2 matrices that describe the unit cell and the coupling between nearest unit cells, respectively. We set $V_0 = 10$ throughout this paper.

Figure 2(b) shows transmission probability $T = |t|^2$ as a function of energy E in a cross-stitch lattice of 100 unit cells with symmetric contacts—that is, $\gamma_a^i = \gamma_b^i = \gamma_a^o = \gamma_b^o = \gamma$, and $t = d = 1$. We set $\gamma = 1$ throughout this paper. The transmission probability corresponds to the dispersive energy bands because the compact localized states in the flatband are such that they are unavailable for transmission. In lattices including both flatbands and dispersive bands, the compact localized part of the lattice related to flatbands can be detangled from the dispersive part of the lattice using a generic transformation [33]. After the transformation, we obtain the dispersive part of the lattice and side-coupled Fano states, where the hopping strength between them is determined by the difference between the on-site potentials of two sites in a unit cell. As a result, if the on-site potentials are symmetric, there is no hopping between the dispersive part of the lattice and the Fano states; thus, the Fano states completely decouple from the dispersive part of the lattice. In this case, the Fano state is the compact localized state of the flatband. Conversely, an asymmetric potential intertwines the dispersive and Fano states. This detangling procedure clearly shows the relation between the local symmetry of the lattice and the compact

localized state, and it explains why the flatband state does not contribute to transmission.

Considering a cross-stitch lattice with symmetric contacts, the amplitude equations of the left end unit cell can be written from Eq. (10) as

$$Ea_1 = \epsilon_a a_1 - a_2 - b_2 - b_1 - \gamma\phi_{-1},$$
$$Eb_1 = \epsilon_b b_1 - b_2 - a_2 - a_1 - \gamma\phi_{-1}, \tag{23}$$

where a_1 and b_1 represent the a and b sites of the left end unit cell, and ϕ_{-1} represents the first site of the left lead. From these equations, we obtain the end unit cell of a lattice with dispersive degrees of freedom p_1 and side-coupled Fano states f_1,

$$Ep_1 = (\epsilon^+ - 1)p_1 + \epsilon^- f_1 - 2p_2 - \sqrt{2}\gamma\phi_{-1},$$
$$Ef_1 = (\epsilon^+ + 1)f_1 + \epsilon^- p_1, \tag{24}$$

where $p_n = (a_n + b_n)/\sqrt{2}$, $f_n = (a_n - b_n)/\sqrt{2}$, $\epsilon^+ = (\epsilon_a + \epsilon_b)/2$, and $\epsilon^- = (\epsilon_a - \epsilon_b)/2$. If $\epsilon^- = 0$, the side-coupled Fano state f_1 becomes a compact localized state of which energy is $\epsilon^+ + 1$ because it is isolated in spite of the coupling between the lattice and leads. In the detangled lattice in the upper panel of Fig. 2(d), the Fano states become compact localized states and do not affect transmission because the Fano states are completely decoupled from the dispersive chain, i.e., $\epsilon^- = 0$.

However, regarding asymmetric contacts, where $\gamma_a^i = \gamma_a^o = \gamma$ and $\gamma_b^i = \gamma_b^o = 0$, a sharp dip in the transmission appears at flatband energy $E = 1$, as shown in Fig. 2(c). This dip in transmission originates from the breaking of local symmetry of the end unit cells due to the asymmetric contacts. When we consider asymmetric contacts, Eq. (24) changes into

$$Ep_1 = (\epsilon^+ - 1)p_1 + \epsilon^- f_1 - 2p_2 - \frac{\gamma}{\sqrt{2}}\phi_{-1},$$

$$Ef_1 = (\epsilon^+ + 1)f_1 + \epsilon^- p_1 - \frac{\gamma}{\sqrt{2}}\phi_{-1}. \quad (25)$$

If $\epsilon^- = 0$, the $f_n(n = 2, \ldots, n - 1)$ inside the lattice are still compact localized states, except for f_1 because of the coupling between f_1 and the lead as shown in the lower panel of Fig. 2(d). The coupling between Fano states and leads due to asymmetric contacts produces the dip in transmission at the flatband energy, although most compact localized states still exist inside the lattice. Considering the amplitude equations for the right unit cell written from Eq. (12), we obtain the same results. It is noted that this transmission dip can also be considered as an antiresonance due to destructive interference, of which position corresponds to the energy of the Fano state [16–19].

B. Tunable diamond lattices

In the case of a tunable diamond lattice, the tight-binding Hamiltonian is given by

$$H_0 = \begin{pmatrix} \epsilon_a & -t & -d \\ -t & \epsilon_b & -d \\ -d & -d & \epsilon_c \end{pmatrix}, \quad H_1 = \begin{pmatrix} 0 & 0 & 0 \\ 0 & 0 & 0 \\ -d & -d & 0 \end{pmatrix}, \quad (26)$$

where $\Psi_j = (a_j b_j c_j)^T$. On-site potential energies are ϵ_a, ϵ_b, and ϵ_c, respectively, and hopping strengths between the sites are d and t. Setting $\Psi_{j+1} = \Psi_j e^{ik}$ and $\Psi_{j-1} = \Psi_j e^{-ik}$ on account of the translational symmetry of the unit cells, we obtain the Hamiltonian for the tunable diamond lattice as

$$H = \begin{pmatrix} \epsilon_a & -t & -d - de^{-ik} \\ -t & \epsilon_b & -d - de^{-ik} \\ -d - de^{ik} & -d - de^{ik} & \epsilon_c \end{pmatrix}. \quad (27)$$

Solving the eigenproblem of H when $\epsilon_a = \epsilon_b = \epsilon_c = 0$, we obtain the energy bands for the tunable diamond lattice as follows:

$$E_{1,2}(k) = -\frac{1}{2}\left(t \pm \sqrt{t^2 + 32d^2 \cos^2 \frac{k}{2}}\right), \quad E_{FB} = t, \quad (28)$$

where $E_{1,2}(k)$ and E_{FB} are dispersive and flatband energies, respectively. Figure 2(e) shows the dispersive and flatbands when $t = d = 1$.

Considering the transport problem in the tunable diamond lattice, $G^{i\,(o)}$ in Eq. (16) changes into

$$G^{i\,(o)} = \begin{pmatrix} -\gamma_a^{i\,(o)} \\ -\gamma_b^{i\,(o)} \\ -\gamma_c^{i\,(o)} \end{pmatrix} \quad (29)$$

and H_0 and H_1 are now 3×3 matrices for the tunable diamond lattice. Figure 2(f) shows transmission $T = |t|^2$ as a function of energy E in a tunable diamond lattice of 100 unit cells with symmetric contacts, e.g., $\gamma_a^i = \gamma_b^i = \gamma_a^o = \gamma_b^o = \gamma$ and $\gamma_c^i = \gamma_c^o = 0$. The transmission probability corresponds to the dispersive energy bands. In the case of asymmetric contacts, where $\gamma_a^i = \gamma_a^o = \gamma$ and $\gamma_b^i = \gamma_b^o = \gamma_c^i = \gamma_c^o = 0$, there is again a dip in transmission at flatband energy $E = 1$, as shown in Fig. 2(g). Transmission in tunable diamond lattices is similar to that in cross-stitch lattices as the detangling of the flatbands is similar, except for the c sites, as shown in Fig. 2(h).

III. QUASI-ONE-DIMENSIONAL LATTICES WITH IMBALANCED ON-SITE POTENTIAL

In this section, we study energy bands and quantum transport in quasi-1D lattices with imbalanced on-site potential. While there are no flatbands in this case, as the symmetry for flatbands is broken by the imbalanced on-site potential, here we are able to find band gaps. We now consider quantum transport in quasi-1D lattices with imbalanced on-site potential. In our case, there is no flatband as the imbalanced potential breaks the flatband and opens up band gaps, as shown in Figs. 3(a) and 4(a).

A. Cross-stitch lattices

To study the effect of imbalanced on-site potential on a cross-stitch lattice, we apply on-site potentials to the diagonal
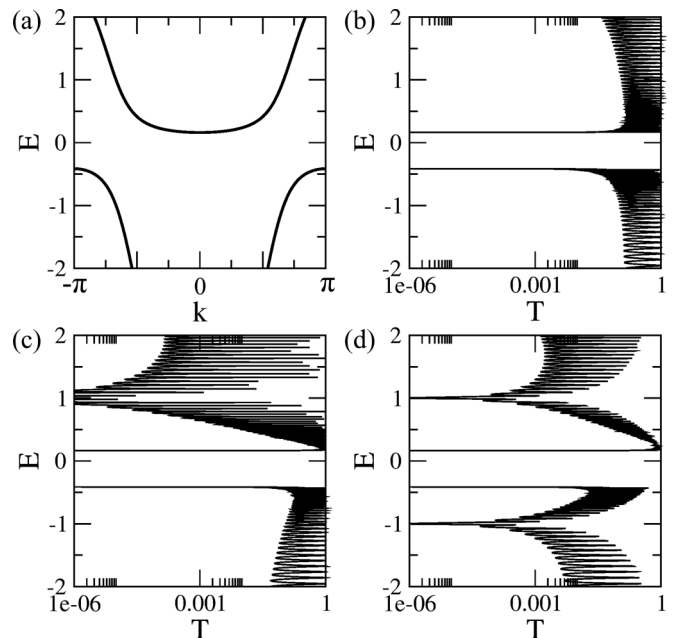

FIG. 3. (a) Energy bands for a cross-stitch lattice with $\delta_a = -2$. (b) Transmission probability for a cross-stitch lattice of which both a and b sites of the end unit cells are connected to the input and output leads. (c) Transmission probability for a cross-stitch lattice of which only the a sites of the end unit cells are connected to the input and output leads. (d) Transmission probability for a cross-stitch lattice of which a and b sites of the end unit cells are connected to the input and the output leads, respectively.
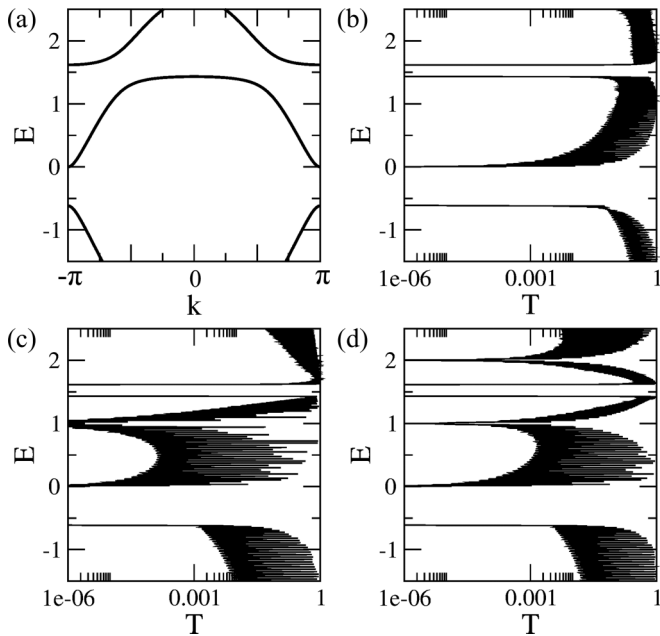
FIG. 4. (a) Energy bands for a tunable diamond lattice with $\delta_a = 1$. (b) Transmission probability for a tunable diamond lattice of which both a and b sites of the end unit cells are connected to the input and output leads. (c) Transmission probability for a tunable diamond lattice of which only the a sites of the end unit cells are connected to the input and output leads. (d) Transmission probability for a tunable diamond lattice of which a and b sites of the end unit cells are connected to the input and the output leads, respectively.

parts of H_0 as follows:

$$H_0 = \begin{pmatrix} \epsilon_0 + \delta_a & -t \\ -t & \epsilon_0 + \delta_b \end{pmatrix}, \tag{30}$$

where δ_a and δ_b are imbalanced on-site potential, or in other words $\delta_a \neq \delta_b$. If we apply imbalanced on-site potential, e.g., $\delta_a = -2$, the two bands exhibit a repulsive behavior that results in a band gap, as seen in Fig. 3(a). In this case, the flatband disappears because the related symmetry is broken.

Figures 3(b)–3(d) shows the transmission probability T when $\delta_a = -2$ and $\epsilon_0 = \delta_b = 0$ in a cross-stitch lattice with different contact configurations. First, we consider that both a and b sites of the end unit cells are connected with the leads. In other words, incident waves from the left lead are transmitted through both a and b sites of the left end unit cell of the lattice to the right lead through both a and b sites of the right end unit cell. In this case, the transmission corresponds with the energy band [cf. Fig. 3(b)]. Second, we consider the case of symmetry-broken contacts, where incident waves from the left lead are transmitted through the left a site of the lattice to the right lead through the right a site. In this case, there exists a dip in transmission at $E = 1$, which is irrelevant to the energy bands of the cross-stitch lattice as well as the energy band gap [cf. Fig. 3(c)]. Finally, we consider the case of different contacts, where incident waves from the left lead are transmitted through the left a site of the lattice to the right lead through the right b site. Here, two dips in transmission appear at $E = 1$ and -1 [cf. Fig. 3(d)]. The last
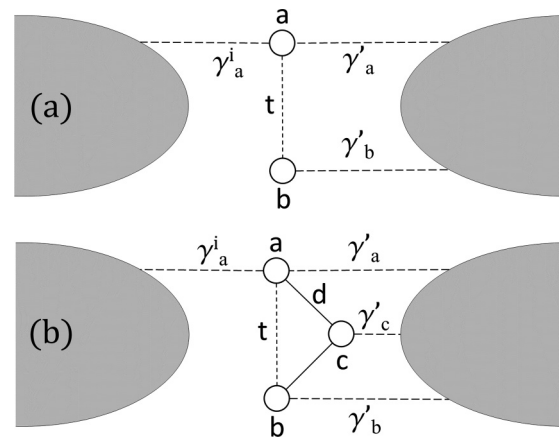

FIG. 5. (a) Schematic diagram of the end unit cells of a cross-stitch lattice connected to the leads. Both a and b sites are connected to the right lead, but only the a site is connected to the left lead. (b) Schematic diagram of the end unit cells of a tunable diamond lattice connected to the leads. All sites are connected to the right lead, but only the a site is connected to the left lead.

two cases of symmetry-broken contacts show additional dips in transmissions that are irrelevant to the energy bands.

To understand the dips in transmission due to symmetry-broken contacts in quasi-1D lattices, which cannot be explained by the energy bands of the lattices, let us reconsider Eq. (5) in detail. The H_{Q1D} term describing the quasi-1D lattices can be divided into two parts, H'_{Q1D} and H_{end}, which represent the flatband excluding the two end unit cells and the two end unit cells, respectively. In this case, H'_{Q1D} precisely describes the band and gap structures of the flatband lattices, as our system is sufficiently large. Therefore, it is H_{end} that produces the additional dips in transmission on account of the asymmetric contacts between the end unit cells and leads. Figure 5(a) depicts a reduced cross-stitch lattice with the asymmetric contacts between leads. When the left lead is connected to the a site only and the right lead is connected to both a and b sites, we can obtain T from the following equation:

$$\begin{pmatrix} -\frac{V_0}{2} \\ \gamma_a^i e^{-iq} \\ 0 \\ 0 \end{pmatrix} = \begin{pmatrix} \frac{V_0}{2} & -\gamma_a^i & 0 & 0 \\ -\gamma_a^i e^{iq} & \epsilon_a - E & -t & -\gamma_a' e^{iq} \\ 0 & -t & \epsilon_b - E & -\gamma_b' e^{iq} \\ 0 & -\gamma_a' & -\gamma_b' & \frac{V_0}{2} \end{pmatrix} \begin{pmatrix} r \\ a \\ b \\ t \end{pmatrix}. \tag{31}$$

For simplicity, if $\gamma_a' = \gamma_b' = \gamma'$, the condition for transmission $T = 0$ is $E_a = \epsilon_b + t$ when the left lead is connected to the a site. Symmetrically, if the left lead is connected to the b site, then the condition is $E_b = \epsilon_a + t$. Finally, with asymmetric contacts, the transmission in Figs. 3(c) and 3(d) dips at $E = E_a$ when the leads are connected to the a site of the end unit cell and at $E = E_b$ for a b-site connection, in addition to the band gaps of the cross-stitch lattice.

These dips in transmission can be considered as antiresonance in terms of the concept of Feynman paths [14,19]. We can obtain the retarded Green's function G_a^r using the Feynman path for electron transmission through the reduced lattice in

Fig. 5(a) as

$$G_a^r = g_a^r - g_a^r t g_b^r + g_a^r t g_b^r t g_a^r - g_a^r t g_b^r t g_a^r t g_a^r + \cdots \quad (32)$$

$$= \frac{g_a^r (1 - t g_b^r)}{1 - t^2 g_a^r g_b^r}, \quad (33)$$

where $g_a^r = 1/(E - \epsilon_a + 2i\Gamma_0)$ and $g_b^r = 1/(E - \epsilon_b + i\Gamma_0)$. The transmission function is associated with Green's function $G_a^r(E)$ by the relation $T(E) \propto |G_a^r(E)|^2$. We can also obtain the condition $E = E_a = \epsilon_b + t$, where the interference of all Feynman paths leads to antiresonance when the left lead is connected to the a site and Γ_0 is infinitesimal.

B. Tunable diamond lattices

Now, to study the effect of imbalanced on-site potential on a tunable diamond lattice, we apply on-site potentials to the diagonal parts of H_0 as follows:

$$H_0 = \begin{pmatrix} \epsilon_0 + \delta_a & -t & -d \\ -t & \epsilon_0 + \delta_b & -d \\ -d & -d & \epsilon_0 + \delta_c \end{pmatrix}, \quad (34)$$

where δ_a, δ_b, and δ_c are imbalanced on-site potential. Under symmetric conditions, e.g., when δ_c is a nonzero real value and $\delta_a = \delta_b = 0$, two dispersive bands show repulsive behavior but the flatband survives. As for asymmetric conditions, e.g., when $\delta_a \neq \delta_b$ and $\delta_c = 0$, the flatbands and the upper dispersive bands demonstrate a repulsive behavior, as shown in Fig. 4(a), because the imbalanced on-site potential breaks the symmetry between the a and b sites, which is the origin of the flatband in the preceding section.

Figures 4(b)–4(d) show the transmission probability T when $\delta_a = 1$ and $\epsilon_0 = \delta_b = \delta_c = 0$ in a tunable diamond lattice with different contact configurations. This case as well presents additional dips in transmission, which can also be understood in the same manner as the former case. When the left lead is connected to the a site only and the right lead is connected to the a, b, and c sites simultaneously, as shown in Fig. 5(b), we can obtain T from the following equation:

$$\begin{pmatrix} -\frac{V_0}{2} \\ \gamma_a^i e^{-iq} \\ 0 \\ 0 \\ 0 \end{pmatrix} = M \begin{pmatrix} r \\ a \\ b \\ c \\ t \end{pmatrix}, \quad (35)$$

where

$$M = \begin{pmatrix} \frac{V_0}{2} & -\gamma_a^i & 0 & 0 & 0 \\ -\gamma_a^i e^{iq} & \epsilon_a - E & -t & -d & -\gamma_a' e^{iq} \\ 0 & -t & \epsilon_b - E & -d & -\gamma_b' e^{iq} \\ 0 & -d & -d & \epsilon_c - E & -\gamma_c' e^{iq} \\ 0 & -\gamma_a' & -\gamma_b' & -\gamma_c' & \frac{V_0}{2} \end{pmatrix}. \quad (36)$$

For simplicity, if $\gamma_a' = \gamma_b' = \gamma_c' = \gamma'$, the condition for transmission $T = 0$ is $E_a = \epsilon_b + t$ or $E_a = \epsilon_c + d$ when the left lead is connected to the a site. As before, a b-site connection gives the condition $E_b = \epsilon_a + t$ or $E_b = \epsilon_c + d$. Finally, with asymmetric contacts, the transmission in Figs. 4(c) and 4(d) dips at $E = E_a$ and $E = E_b$ when the lead is connected to the a site and the b site of the end unit cell, respectively. These dips in transmission can also be considered as antiresonance in terms of the Feynman path; the former condition, $E_a = \epsilon_b + t$, can be obtained from the same Feynman paths as those in the cross-stitch lattice if we consider the Feynman paths including only a and b sites, exclusive of the c site, in Fig. 5(b). Similarly, the latter condition $E_a = \epsilon_c + d$ can be obtained from the Feynman paths, which include the a and c sites but exclude the b site. As seen in Fig. 4, there are multiple antiresonances in the tunable diamond lattice.

IV. DISCUSSION AND SUMMARY

In principle, our results demonstrating that the contacts between a system and leads can induce various resonant phenomena can be applied to quantum transport in diverse situations, e.g., in the presence of defects and flatbands [16–19,34]. If the contact does not break the intrinsic properties of the system, such as the parity symmetry of a quasi-1D lattice, then the contact does not influence quantum transport. In the case of a symmetry-broken contact, however, antiresonance indirectly reflects nonmobile states as compact localized states, since the contact perturbs one of the flatband states at the edge of the system. As a result, contact configurations that break the symmetries that determine the intrinsic properties of a quantum state play an important role in transport.

In summary, we have studied quantum transport in quasi-one-dimensional lattices with symmetric and asymmetric contacts. In a quasi-1D lattice with balanced on-site potential, flatbands can be detected through asymmetric rather than symmetric contacts, and in a lattice with imbalanced on-site potential, transmission was suppressed at certain energies in the case of asymmetric contacts. We have elucidated the energies of the transmission suppressions related to antiresonance using reduced lattice models and Feynman paths. There is no overlap between compact localized states of a flatband because the states have nonzero amplitude only at a finite number of lattice sites. Consequently, it is very difficult to detect flatband energy in quantum transport because compact localized states do not contribute to the transport. Due to the isolation of compact localized states, however, asymmetric contacts facilitate a nondestructive measurement of flatband energy.

[1] M. A. Kastner, Phys. Today **46**(1), 24 (1993).

[2] R. C. Ashoori, Nature (London) **379**, 413 (1996).

[3] A. W. Holleitner, C. R. Decker, H. Qin, K. Eberl, and R. H. Blick, Phys. Rev. Lett. **87**, 256802 (2001).

[4] A. W. Holleitner, R. H. Blick, A. K. Huttel, K. Eberl, and J. P. Kotthaus, Science **297**, 70 (2002).

[5] W. Z. Shangguan, T. C. Au Yeung, Y. B. Yu, and C. H. Kam, Phys. Rev. B **63**, 235323 (2001).

[6] F. R. Braakman, P. Barthelemy, C. Reichl, W. Wegscheider, and L. M. K. Vandersypen, Nat. Nanotech. **8**, 432 (2013).

[7] T. Hensgens, T. Fujita, L. Janssen, X. Li, C. J. Van Diepen, C. Reichl, W. Wegscheider, S. Das Sarma, and L. M. K. Vandersypen, Nature (London) **548**, 70 (2017).

[8] T. Nakajima, M. R. Delbecq, T. Otsuka, P. Stano, S. Amaha, J. Yoneda, A. Noiri, K. Kawasaki, K. Takeda, G. Allison, A. Ludwig, A. D. Wieck, D. Loss, and S. Tarucha, Phys. Rev. Lett. **119**, 017701 (2017).

[9] B. Zhen, C. W. Hsu, Y. Igarashi, L. Lu, I. Kaminer, A. Pick, S.-L. Chua, J. D. Joannopoulos, and M. Soljacic, Nature (London) **525**, 354 (2015).

[10] F. Baboux, L. Ge, T. Jacqmin, M. Biondi, E. Galopin, A. Lemaítre, L. Le Gratiet, I. Sagnes, S. Schmidt, H. E. Türeci, A. Amo, and J. Bloch, Phys. Rev. Lett. **116**, 066402 (2016).

[11] A. Cerjan, A. Raman, and S. Fan, Phys. Rev. Lett. **116**, 203902 (2016).

[12] K. Esaki, M. Sato, K. Hasebe, and M. Kohmoto, Phys. Rev. B **84**, 205128 (2011).

[13] T. E. Lee, Phys. Rev. Lett. **116**, 133903 (2016).

[14] S. Datta, *Electron Transport in Mesoscopic Systems* (Cambridge University Press, Cambridge, UK, 1997).

[15] D. A. Ryndyk, *Theory of Quantum Transport at Nanoscale: An Introduction* (Springer International, Cham, Switzerland, 2016).

[16] X. R. Wang, Y. Wang, and Z. Z. Sun, Phys. Rev. B **65**, 193402 (2002).

[17] P. A. Orellana, F. Domínguez-Adame, I. Gómez, and M. L. Ladrón de Guevara, Phys. Rev. B **67**, 085321 (2003).

[18] P. A. Orellana, M. L. Ladrón de Guevara, M. Pacheco, and A. Latgé, Phys. Rev. B **68**, 195321 (2003).

[19] K. Bao and Y. Zheng, Phys. Rev. B **73**, 045306 (2006).

[20] A. Simon, Angew. Chem. **109**, 1873 (1997).

[21] S. Deng, A. Simon, and J. Köhler, Angew. Chem. **110**, 664 (1998).

[22] M. Imada and M. Kohno, Phys. Rev. Lett. **84**, 143 (2000).

[23] S. Deng, A. Simon, and J. Köhler, J. Solid State Chem. **176**, 412 (2003).

[24] V. Apaja, M. Hyrkäs, and M. Manninen, Phys. Rev. A **82**, 041402(R) (2010).

[25] M. Hyrkäs, V. Apaja, and M. Manninen, Phys. Rev. A **87**, 023614 (2013).

[26] M. C. Rechtsman, J. M. Zeuner, A. Tünnermann, S. Nolte, M. Segev, and A. Szameit, Nat. Photon. **7**, 153 (2013).

[27] R. A. Vicencio, C. Cantillano, L. Morales-Inostroza, B. Real, C. Mejía-Cortés, S. Weimann, A. Szameit, and M. I. Molina, Phys. Rev. Lett. **114**, 245503 (2015).

[28] S. Mukherjee, A. Spracklen, D. Choudhury, N. Goldman, P. Öhberg, E. Andersson, and R. R. Thomson, Phys. Rev. Lett. **114**, 245504 (2015).

[29] T. Jacqmin, I. Carusotto, I. Sagnes, M. Abbarchi, D. D. Solnyshkov, G. Malpuech, E. Galopin, A. Lemaitre, J. Bloch, and A. Amo, Phys. Rev. Lett. **112**, 116402 (2014).

[30] O. Derzhko and J. Richter, Eur. Phys. J. B **52**, 23 (2006).

[31] D. L. Bergman, C. Wu, and L. Balents, Phys. Rev. B **78**, 125104 (2008).

[32] O. Derzhko, J. Richter, A. Honecker, M. Maksymenko, and R. Moessner, Phys. Rev. B **81**, 014421 (2010).

[33] S. Flach, D. Leykam, J. D. Bodyfelt, P. Matthies, and A. S. Desyatnikov, Europhys. Lett. **105**, 30001 (2014).

[34] A. A. Lopes, B. A. Z. António, and R. G. Dias, Phys. Rev. B **89**, 235418 (2014).